7-8-2024

Patient-specific quality assurance of dynamically-collimated proton therapy treatment plans

Alonso Gutierrez
Miami Cancer Institute, alonsog@baptisthealth.net

Eduardo Pons
Miami Cancer Institute, Eduardo.Pons@baptisthealth.net

Andrew Wroe
Miami Cancer Institute, AndrewWr@baptisthealth.net

Citation
Medical Physics (2024) [Epub ahead of print] Published online July 8

Received: 12 March 2024 | Revised: 16 May 2024 | Accepted: 10 June 2024

DOI: 10.1002/mp.17295

RESEARCH ARTICLE

MEDICAL PHYSICS

Patient-specific quality assurance of dynamically-collimated proton therapy treatment plans

Laura C. Bennett[1] | **Daniel E. Hyer**[2] | **Justin Vu**[1] | **Kaustubh Patwardhan**[2] | **Kevin Erhart**[3] | **Alonso N. Gutierrez**[4] | **Eduardo Pons**[4] | **Eric Jensen**[5] | **Manual Ubau**[5] | **Julio Zapata**[5] | **Andrew Wroe**[4] | **Karsten Wake**[6] | **Nicholas P. Nelson**[6,7] | **Wesley S. Culberson**[6] | **Blake R. Smith**[2] | **Patrick M. Hill**[8] | **Ryan T. Flynn**[2]

[1]Roy J. Carver Department of Biomedical Engineering, University of Iowa, 5601 Seamans Center for the Engineering Arts and Sciences, Iowa City, Iowa, USA

[2]Department of Radiation Oncology, University of Iowa Hospitals and Clinics, Iowa City, Iowa, USA

[3].decimal LLC, Sanford, Florida, USA

[4]Department of Radiation Oncology, Miami Cancer Institute, Baptist Health South Florida, Miami, Florida, USA

[5]Ion Beam Applications S.A., R&D Proton Therapy, Louvain-La-Neuve, Belgium

[6]Department of Medical Physics, School of Medicine and Public Health, University of Wisconsin, Madison, Wisconsin, USA

[7]Department of Radiation Oncology, Huntsman Cancer Institute, University of Utah, Salt Lake City, Utah, USA

[8]Department of Human Oncology, School of Medicine and Public Health, University of Wisconsin, Madison, Wisconsin, USA

Correspondence
Laura C. Bennett, Roy J. Carver Department of Biomedical Engineering, University of Iowa, Iowa City, IA 52242, USA.
Email: laura-bennett@uiowa.edu

Funding information
National Cancer Institute; National Institutes of Health, Grant/Award Number: R37CA226518

Abstract

Background: The dynamic collimation system (DCS) provides energy layer-specific collimation for pencil beam scanning (PBS) proton therapy using two pairs of orthogonal nickel trimmer blades. While excellent measurement-to-calculation agreement has been demonstrated for simple cube-shaped DCS-trimmed dose distributions, no comparison of measurement and dose calculation has been made for patient-specific treatment plans.

Purpose: To validate a patient-specific quality assurance (PSQA) process for DCS-trimmed PBS treatment plans and evaluate the agreement between measured and calculated dose distributions.

Methods: Three intracranial patient cases were considered. Standard uncollimated PBS and DCS-collimated treatment plans were generated for each patient using the Astroid treatment planning system (TPS). Plans were recalculated in a water phantom and delivered at the Miami Cancer Institute (MCI) using an Ion Beam Applications (IBA) dedicated nozzle system and prototype DCS. Planar dose measurements were acquired at two depths within low-gradient regions of the target volume using an IBA MatriXX ion chamber array.

Results: Measured and calculated dose distributions were compared using 2D gamma analysis with 3%/3 mm criteria and low dose threshold of 10% of the maximum dose. Median gamma pass rates across all plans and measurement depths were 99.0% (PBS) and 98.3% (DCS), with a minimum gamma pass rate of 88.5% (PBS) and 91.2% (DCS).

Conclusions: The PSQA process has been validated and experimentally verified for DCS-collimated PBS. Dosimetric agreement between the measured and calculated doses was demonstrated to be similar for DCS-collimated PBS to that achievable with noncollimated PBS.

KEYWORDS
collimation, dose calculation, dynamic collimation system (DCS), dynamic collimation, pencil beam scanning (PBS), proton therapy, spot scanning

1 | INTRODUCTION

Pencil beam scanning (PBS) proton therapy combines the ability of therapeutic proton beams to provide distal dose shaping via energy selection with the use of upstream scanning magnets to magnetically steer the beam and provide lateral dose conformity around the target volume.[1–4] The increased spot sizes that occur at the lower energies required to treat shallow targets in the brain and head-and-neck, often result in reduced lateral dose conformity and subsequently lower plan quality.[5,6] This effect is exacerbated with the use of range shifters and extended air gaps required for clearance with some patient anatomy. To combat this, external collimation may be indicated for use in PBS proton therapy.

One device designed for this purpose is the dynamic collimation system (DCS). The DCS provides spot-by-spot collimation for PBS to improve lateral dose conformity for shallow targets without compromising the dose to the target.[7,8] Beams are collimated using two pairs of focused orthogonal trimmer blades of 3 cm thickness to reduce transmission of beams throughout the intended energy range of the DCS and made of nickel to reduce secondary neutron production.[9,10] In silico treatment planning studies have demonstrated that the device is capable of delivering more conformal plans compared to traditional PBS treatments,[11–16] and a prototype of the device has been dosimetrically validated with physical measurements of simplistic phantom plans that were performed at the Miami Cancer Institute (MCI) using an IBA dedicated PBS nozzle system.[15,16] Following the recent development and integration of the DCS beam model into the commercial treatment planning system (TPS) Astroid,[17] it is necessary to establish a patient-specific quality assurance (PSQA) process to enable patient treatments with the DCS. In this work, an approach to PSQA with the DCS is described and evaluated by measurement for treatment plans generated both with and without the DCS in the Astroid TPS.

2 | MATERIALS AND METHODS

2.1 | Treatment planning

For this study, uncollimated PBS plans were generated for three patients with tumors in the brain that were previously treated with proton therapy. All plans had three-beam arrangements with beam angles nominally chosen to minimize the distance between surface and target, avoid large density heterogeneities, and prevent end-ranging in critical structures. Spots were initialized on a hexagonal grid with 4 mm lateral and distal margins around the target with lateral spacing of 0.7σ (in-air spot size at isocenter) and distal spacing of half the width of the Bragg peak as measured from the proximal to distal locations of the 80% maximum dose on the integral depth dose (IDD) curve. The Astroid TPS allows planners to select unique dose grid sizes for different structures to enhance calculation speed while providing increased resolution and accuracy for smaller or more critical structures. Structures for which the dose grid size is not explicitly defined use a default base dose grid that is unique for each plan. For this study, the base dose grid for all patients was 4 mm, with select structures such as the target and nearby organs at risk (OAR) having a reduced dose grid size of 1 or 2 mm to improve dose calculation accuracy. A summary of the patient diagnoses, target volumes, prescription doses, and beams used is shown in Table 1.

For all plans, treatment planning was completed in the Astroid TPS, an FDA-cleared system (.decimal, Sanford, FL, USA). Constraints and planning objectives for all plans were chosen in accordance with recommendations provided by results from the Quantitative Analysis of Normal Tissue Effects in the Clinic (QUANTEC) program.[18,19] A constraint of $V_{95\%} = 100\%$ for the planning target volume (PTV) was applied for all treatment plans, where $V_{95\%}$ is the volume receiving 95% of the prescription dose, D_P. This ensures that 100% of the targeted volume receives a minimum of 95% of the planned radiation dose The maximum dose constraint, $D_{\max}$, for all plans was 110% of D_P. A ring structure was created around the target delineating the normal tissue within a 10 mm radius from the target edge in each direction. The mean dose to the ring $\bar{D}$ was calculated for each patient plan to evaluate dose falloff and normal tissue sparing around the target. In addition, the Dose Gradient Index (DGI), defined as the ratio of the volume encompassed by the 50% prescription isodose line and the 100% isodose line, was calculated to compare overall dose falloff among plans.[20]

Plans were optimized using a multi-field optimization (MFO) approach using the ART3+O algorithm to perform multi-criteria optimization (MCO).[21] Following the successful construction of a database of Pareto-optimal plans, the Pareto space of plans was navigated to minimize mean dose to the 1 cm ring around the target volume without compromising the target coverage requirement.

2.2 | DCS planning

Once the uncollimated PBS plan was finalized for a patient, the plan was exported to a MATLAB-based plugin, hereafter referred to as HybridTrim (HT). Beam angles, beam energy, spot coordinates, patient structure coordinates, and the relative stopping power grid for the patient were used to generate an initial set of DCS trimmer positions based on the methods of Smith et al.[22]

TABLE 1 Description of patient cases, prescription doses, and beam orientation/energy.

Patient number	Diagnosis	Target volume (cm^3)	Prescription dose (Gy [RBE])	Beam orientation (Gantry, Couch)	Energy range (Min MeV, Max MeV)
1	Meningioma	32.4	54	(50°, 0°)	(71.0, 126.9)
				(90°, 0°)	(71.4, 127.1)
				(60°, −90°)	(100.0, 159.5)
2	Craniopharyngioma	91	54	(310°, 90°)	(71.6, 131.4)
				(270°, 0°)	(70.9, 106.9)
				(270°, −30°)	(71.4, 122.9)
3	Chordoma	42	50	(230°, −15°)	(71.9, 128.8)
				(270°, 55°)	(82.6, 120.0)
				(300°, −30°)	(71.5, 118.4)

Abbreviation: RBE, relative biological effectiveness.

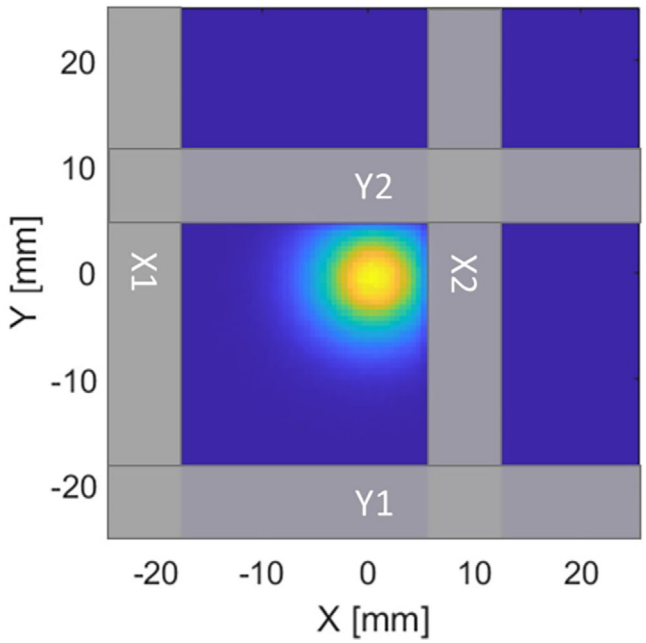

FIGURE 1 Proton spot being collimated by DCS trimmers (shown in gray), with *X*2 and *Y*2 trimmers serving as dominant trimmers. DCS, dynamic collimation system.

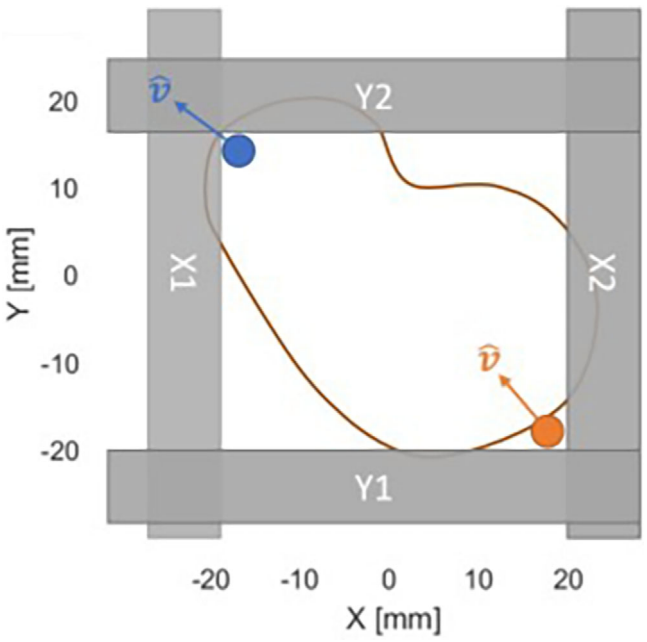

FIGURE 2 The value of $\hat{v}$ for spots located outside of the target (orange) is calculated with respect to the proximity of the spot to target voxels. Conversely, the value of $\hat{v}$ for spots located inside the target (blue) is calculated with respect to the proximity of the spot to normal tissue voxels. In the above example, the dominant trimmers for the external spot are *X*2 and *Y*1. For the internal spot, the dominant trimmers are *X*1 and *Y*2.

For each spot, a single orthogonal pair of trimmers were chosen to be the dominant trimmers for that spot and were initialized at the tightest allowed degree of collimation, defined as 0.5 mm between the medial edge of the trimmer and the spot centroid at isocenter. The remaining two trimmers were initialized such that they had no impact on the lateral dose distribution of the spot (Figure 1).

The location of the spot's central axis relative to the target determined which two trimmers to designate as dominant at the point of initialization. For spots located outside of the target, the dominant trimmers were chosen to maximize the dose inside the target by calculating a unit vector $\hat{v}$ to estimate the direction of the majority of target voxels in proximity to the spot. The sign of $\hat{v}$ in each dimension was used to determine the dominant trimmer in *X* and *Y*, with negative values associated with the *X*1/*Y*1 trimmers and positive values the *X*2/*Y*2 trimmers. For spots located inside the target, the dominant trimmers were chosen to minimize dose outside of the target and the unit vector $\hat{v}$ was calculated to estimate the direction of the majority of normal tissue voxels. The sign of $\hat{v}$ was used to determine the dominant trimmers in a similar manner to external spots, but with negative values associated with *X*2/*Y*2 trimmers and positive values the *X*1/*Y*1 trimmers. Figure 2 depicts an example of how $\hat{v}$ was used to determine dominant trimmers for spots both inside and outside of the target.

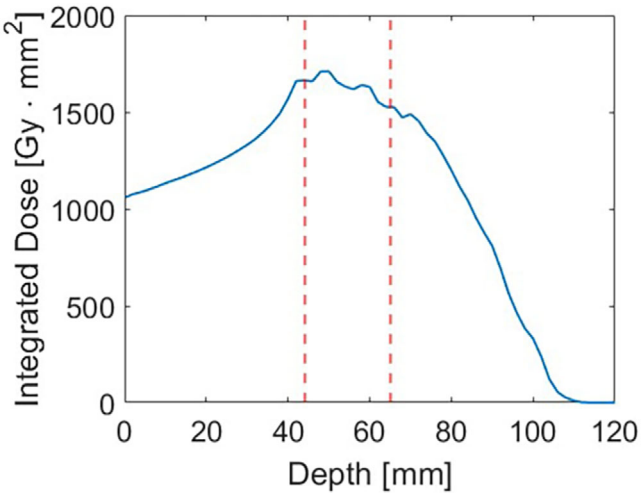

FIGURE 3 Measurement depths were selected in regions of both high-dose and low-dose gradient in the proximal/distal direction. The depth dose along the central axis of the fractional dose of one DCS field for Patient 2 is depicted here (solid blue line) along with two selected measurement depths (dashed red lines). DCS, dynamic collimation system.

After the dominant trimmers were assigned, the spots were grouped into layers according to the methods outlined by Smith et al.[23] to improve delivery efficiency. The new spot groups were then exported out of HT and imported back into the Astroid TPS environment, where the same constraints and objectives used to create the PBS plan were used to optimize beamlet intensities for the trimmed spots and generate a DCS plan with comparable target coverage and mean target dose.

2.3 | PSQA delivery and analysis

Following the completion of treatment planning, optimized plans were recalculated within a water phantom with a dose grid size of $2 \times 2 \times 2$ mm^3 to balance computational efficiency and accuracy.[24–26] They were delivered at the MCI using the IBA Proteus Plus system (Ion Beam Applications SA, Louvain-la-Neuve, Belgium) with the DCS mounted to the end of the IBA Dedicated Nozzle (DN). All plans were calculated and delivered with the isocenter positioned at the phantom surface. An air gap of 7 cm was maintained between the phantom surface and the downstream edge of the X trimmers of the DCS. Planar dose was captured at two depths per beam using the IBA DigiPhant in combination with the IBA MatriXX PT ionization chamber array (IBA Dosimetry, Germany). Measurement depths were selected using the depth dose profiles along the central axis of the beams of calculated distributions to find regions of both high dose and low proximal/distal dose gradients (Figure 3). To evaluate agreement between calculated and measured dose distributions, planar gamma analysis was performed with a global 3%/3 mm criterion and low dose threshold of 10% of the maximum dose in accordance with clinical PSQA criteria at MCI as well as those of other institutions and recommendations from the AAPM.[24,25,27–32] This criterion was also chosen to account for uncertainties in the measurement setup of 1% of the dose based on measurement against a known standard and spatial uncertainty of 1 mm when using the kV imager. In accordance with MCI PSQA standards, a field was considered to "pass" if at least 90% of evaluated points at the depth measured met the aforementioned criteria. A Wilcoxon rank sum test was performed on the gamma pass rates for DCS and PBS measurements to establish if there was a statistically significant difference between the two groups.[33] This test was selected assuming the distributions in gamma pass rates were non-parametric, and the measurements were independent, as DCS and PBS plans had different spot arrangements and measurements occurred at different depths. In addition to the gamma pass rates, per-field delivery times and monitor units (MU) were extracted from the IBA log files for further analysis.

2.4 | MatriXX-PT suitability for DCS PSQA

The IBA MatriXX-PT is well established for PSQA of standard PBS proton therapy.[32,34,35] The MatriXX-PT has 1020 ion chambers with 2 mm electrode spacing offering measurement uncertainties of $< 1\%$,[34] with center-to-center chamber spacing of 7.6 mm, and chamber diameters of 3.8 mm. A vendor-supported approach to improve measurement resolution is to obtain two acquisitions of each proton therapy field, one with the array at the nominal position, and one with the array shifted 3.8 mm in both the vertical and horizontal directions, resulting in a final measurement grid spacing of 5.4 mm. To assess the suitability of the MatriXX-PT system for DCS PSQA, an exhaustive induced-error analysis was performed with proposed PSQA failure criteria of less than 90% of the pixels receiving above 10% of the maximum dose for a given measurement passing the gamma criterion at the 3%/3 mm level. This was accomplished by defining the error vector $\vec{e}_i = (\Delta x_i, \Delta y_i, \Delta d_i)$, where $\Delta x = (-4, -3, -2, -1, 0, 1, 2, 3, 4)$ (mm) represents a dose distribution shift in the x-direction (parallel to the MatriXX-PT detector array), $\Delta y = (-4, -3, -2, -1, 0, 1, 2, 3, 4)$ (mm) represents a dose distribution shift in the y-direction (parallel to the MatriXX-PT detector array), and $\Delta d = (-4, -3, -2, -1, 0, 1, 2, 3, 4)$ (%) is the percent change in dose, and $i = 1, \ldots, 9^3 = 729$ is the shift index that identifies all possible combinations of $\Delta x_i, \Delta y_i,$ and Δd_i values. For each calculated 2-D

TABLE 2 Selected DVH metrics for each patient and plan.

Structure evaluated	Metric (Units)	Patient 1			Patient 2			Patient 3		
		PBS	DCS	%Δ	PBS	DCS	%Δ	PBS	DCS	%Δ
Target	$V_{100\%}$(%)	95.6%	95.4%	0.209%	95.2%	95.2%	0.00%	95.4%	95.3%	0.105%
–	DGI (–)	3.68	3.12	16.5%	2.76	2.33	16.9%	3.53	3.21	9.50%
Ring	$\bar{D}$ (Gy [RBE])	43.1	33.8	24.2%	36.6	31.3	14.8%	35.5	30.4	15.5%

Abbreviations: DCS, dynamic collimation system; DGI, dose gradient index; PBS, pencil beam scanning; RBE, relative biological effectiveness.

TABLE 3 Minimum, maximum, and mean doses for select OARs for all patients and plans as a percentage of prescription dose.

Structure evaluated	Metric	Patient 1			Patient 2			Patient 3		
		PBS	DCS	Δ	PBS	DCS	Δ	PBS	DCS	Δ
Brainstem	D_{min}	0.00%	0.00%	0.00%	0.00%	0.00%	0.00%	0.00%	0.00%	0.00%
	D_{max}	105.60%	106.30%	0.70%	104.40%	104.60%	0.20%	106.00%	106.40%	0.40%
	$\bar{D}$	46.11%	37.22%	–8.89%	44.26%	40.74%	–3.52%	24.20%	19.88%	–4.32%
Optic chiasm	D_{min}	39.07%	31.30%	–7.77%	80.19%	76.85%	–3.34%	0.91%	0.00%	–0.91%
	D_{max}	100.70%	101.50%	0.80%	102.60%	103.50%	0.90%	105.00%	106.20%	1.20%
	$\bar{D}$	90.00%	81.85%	–8.15%	99.26%	99.81%	0.55%	60.80%	52.60%	–8.20%
Left cochlea	D_{min}	82.59%	64.81%	–17.78%	–	–	–	–	–	–
	D_{max}	104.30%	104.60%	0.30%	–	–	–	–	–	–
	$\bar{D}$	98.33%	95.00%	–3.33%	–	–	–	–	–	–
Left eye	D_{min}	0.00%	0.00%	0.00%	–	–	–	–	–	–
	D_{max}	12.30%	12.93%	0.63%	–	–	–	–	–	–
	$\bar{D}$	2.06%	0.59%	–1.47%	–	–	–	–	–	–
L. Optic nerve	D_{min}	5.65%	0.70%	–4.95%	0.56%	0.02%	–0.54%	0.06%	0.04%	–0.02%
	D_{max}	104.30%	104.40%	0.10%	89.81%	90.37%	0.56%	14.00%	7.16%	–6.84%
	$\bar{D}$	53.89%	40.93%	–12.96%	22.59%	15.22%	–7.37%	4.72%	2.36%	–2.36%
R. Optic nerve	D_{min}	0.000%	0.000%	0.000%	16.26%	6.22%	-10.04%	1.19%	0.04%	–1.15%
	D_{max}	102.40%	104.10%	1.70%	102.80%	103.90%	1.10%	103.60%	106.20%	2.60%
	$\bar{D}$	31.11%	25.00%	–6.11%	80.56%	75.93%	–4.63%	39.00%	31.40%	–7.60%
L. Temp. Lobe	D_{min}	0.00%	0.00%	0.00%	–	–	–	–	–	–
	D_{max}	104.63%	105.19%	0.56%	–	–	–	–	–	–
	$\bar{D}$	28.89%	22.04%	–6.85%	–	–	–	–	–	–
Pituitary	D_{min}	–	–	–	57.59%	54.07%	–3.52%	36.60%	16.86%	–19.74%
	D_{max}	–	–	–	101.90%	103.30%	1.40%	98.80%	99.20%	0.40%
	$\bar{D}$	–	–	–	87.41%	86.11%	–1.30%	62.60%	51.60%	–11.00%

Note: Structures receiving zero dose for a given patient are not tabulated.
Abbreviations: DCS, dynamic collimation system; OARs, organs at risks; PBS, pencil beam scanning.

dose distribution corresponding to a PSQA measurement (36 for PBS and 36 for DCS), the calculated dose distribution was resampled onto the 5.4 mm MatriXX-PT array grid and then interpolated onto a 2 mm × 2 mm spatial grid, representing a virtual measurement. All 729 combinations of $\vec{e}_i$-vectors were applied to each virtual measurement to simulate shifts and dose scaling operations, and, for each of those, the gamma test was run, resulting in a total of $2 \cdot 36 \cdot 729 = 52\,488$ simulated PSQA tests with the MatriXX-PT system. For all 2-D dose distributions considered for measurement, the minimum $|\vec{e}_i|$-values for which the gamma test failed for PBS and DCS were 3.11 and 3.01, respectively, indicating no substantial difference between the PSQA approach proposed for PBS and DCS, despite the higher dose gradients present with the DCS. This indicates the proposed approach of using the MatriXX PT for DCS PSQA using the proposed gamma passage criteria is as appropriate as using the same approach for PBS, which is already an established approach.[32,34,35]

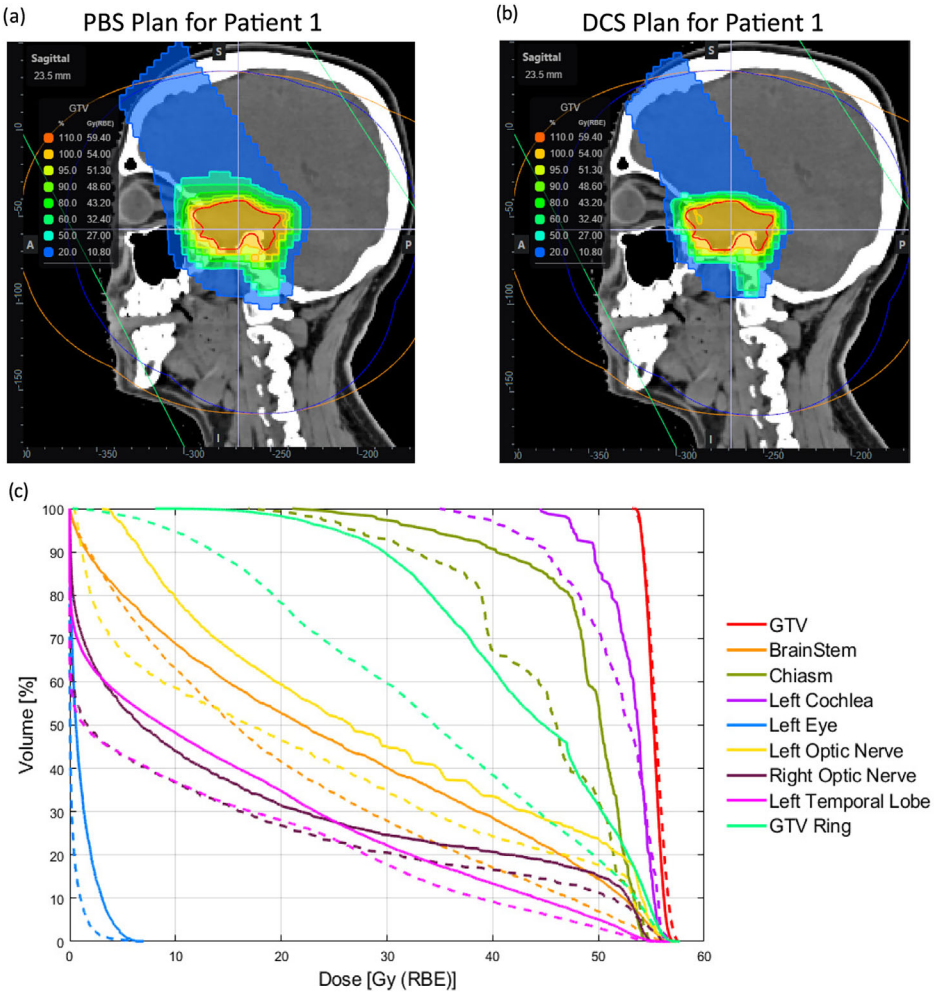

FIGURE 4 Treatment planning results for Patient 1. (a) Isodose distribution and gross tumor volume (GTV) (outlined in red) for PBS plan. (b) Isodose distribution and GTV for DCS plan. (c) DVH for both the PBS plan shown in (a) (solid lines) and DCS plan in (b) (dashed lines). DCS, dynamic collimation system; PBS, pencil beam scanning.

3 | RESULTS

3.1 | Treatment planning results

All plans met the minimum target dose criteria with $V_{95\%}$ = 100% and no plans exceeded the maximum target dose criteria of 110% of D_P. The maximum target dose amongst all plans was 107.7% for PBS plans and 107.4% for DCS plans. The $V_{100\%}$, DGI, and median dose to the 10 mm ring around the target are summarized for each patient and plan in Table 2, and OAR doses as a percentage of prescription dose are tabulated in Table 3. A sample dose volume histogram (DVH) plot and associated dose distributions for Patient 1 are shown in Figure 4.

3.2 | PSQA measurements

For all beams, all but one measurement passed the minimum gamma threshold of 90% using gamma criteria of 3%/3 mm with a low dose threshold of 10% of the maximum dose. Median pass rates between PBS and DCS fields were similar at 99% (PBS) and 98.3% (DCS), with minimum pass rates at 88.5% (PBS) and 91.2% (DCS). The difference in gamma pass rates for all measurements between the two groups was not statistically significant according to a Wilcoxon rank sum test (p = 0.14). A sample comparison for one patient is depicted in Figure 5, and a summary of gamma pass rates across all measurements for each patient is shown in Table 4. The distribution of gamma pass rates is also summarized in Figure 6.

3.3 | Delivery comparison

The median delivery time for DCS fields was longer than standard PBS fields at 106.8 s for PBS and 201.0 s for DCS fields. Additionally, the spread of delivery times was greater for DCS fields (IQR = 63.4 s) compared to PBS fields (IQR = 12.0 s). For the DCS

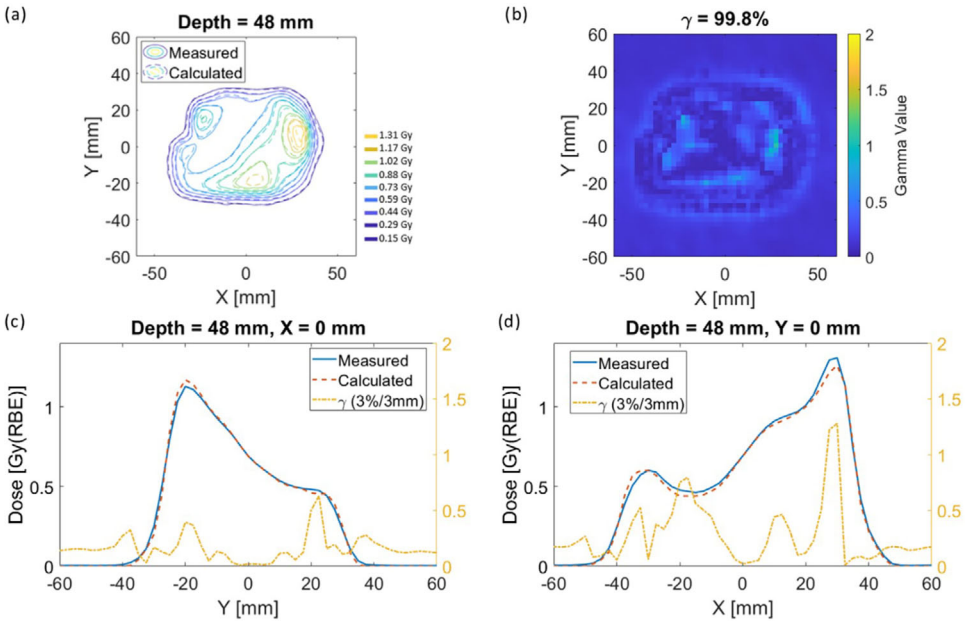

FIGURE 5 Comparison of calculated and measured dose distributions for one DCS field at a depth of 48 mm for Patient 2. Dose values listed represent the relative biological effectiveness (RBE)-scaled dose. (a) Isodose contours from 10% to 100% the maximum measured dose for this field at this depth. (b) 3%/3 mm gamma analysis of the same field at the same depth. (c) $X = 0$ line profile comparison of calculated and measured dose distributions at 48 mm depth. (d) $Y = 0$ line profile comparison of calculated and measured dose distributions at 48 mm depth. DCS, dynamic collimation system.

TABLE 4 Summary of gamma passing rates across all beams and measurement depths for each patient.

		Patient 1	Patient 2	Patient 3	Overall
Mean	PBS	99.0%	96.9%	99.1%	98.3%
	DCS	97.4%	98.7%	96.1%	96.9%
Median	PBS	98.9%	98.5%	99.0%	99.0%
	DCS	98.4%	99.4%	97.1%	98.3%
Minimum	PBS	97.5%	88.5%	98.0%	88.5%
	DCS	91.8%	95.5%	91.2%	91.2%

Note: Gamma criteria was 3%/3 mm with 10% maximum dose threshold.
Abbreviations: DCS, dynamic collimation system; PBS, pencil beam scanning.

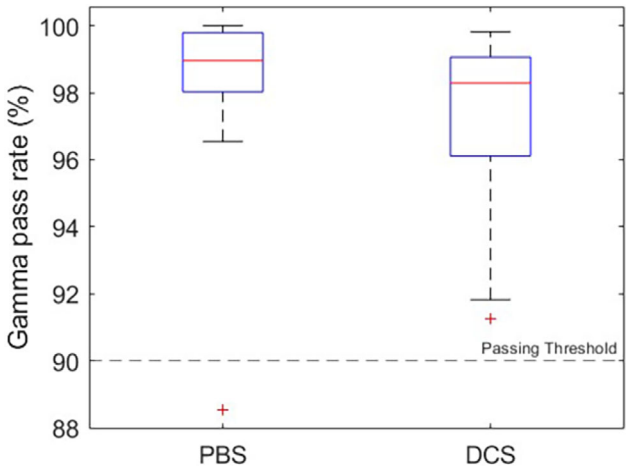

FIGURE 6 Distribution of gamma pass rates for all beams and measurement depths at the 3%/3 mm gamma criteria. Outliers are depicted as red crosses. The minimum threshold for a measurement to pass is depicted at 90%.

plans, longer delivery times were observed for fields that had a larger number of unique trimmer positions. The difference in delivery times between PBS and DCS plans as well as between DCS fields with different numbers of unique trimmer positions is summarized in Figure 7.

The number of MU per field was also generally greater for DCS plans. The median number of MU across all fields was 31.6% higher for DCS fields (130.45 MU) when compared with the median number of MU for PBS fields (94.87 MU). The difference in MU between DCS and PBS plans on a per-field basis was not statistically significant when compared using a Wilcoxon rank sum test ($p = 0.22$). The distribution of total MU for PBS and DCS across all patients and fields is summarized in Figure 8.

The total number of MU for a given plan, defined as the sum of MU for each beam, was uniformly higher for DCS plans compared to PBS plans with an average increase of 22.3%. The difference in per-beam and total MU for each patient is depicted in Figure 9.

4 | DISCUSSION

Gamma pass rates tended to be slightly higher for PBS measurements compared to DCS measurements;

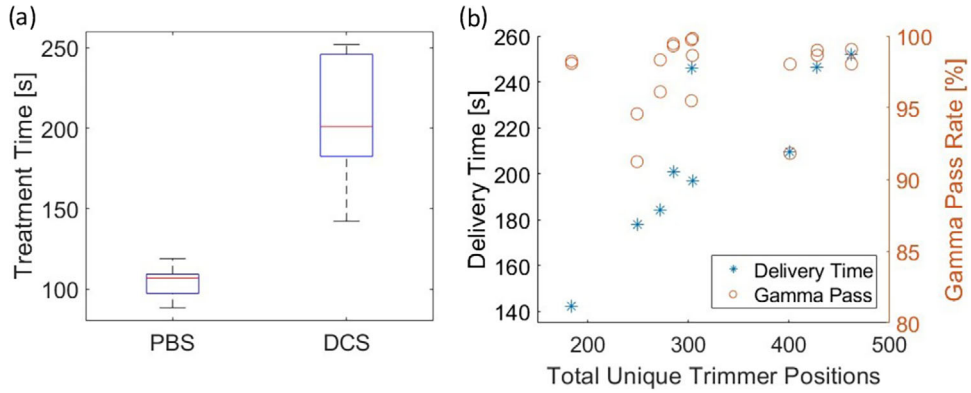

FIGURE 7 (a) Comparison of per-field delivery times between PBS (left) and DCS (right) plans. (b) Delivery time and gamma pass rate versus total trimmer positions per field for DCS deliveries. DCS, dynamic collimation system; PBS, pencil beam scanning.

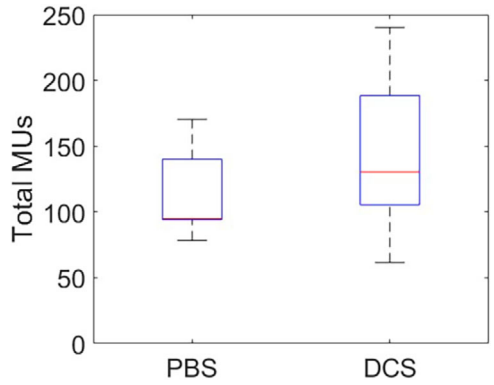

FIGURE 8 Distribution of total MU per field for PBS (left) and DCS (right) beams. DCS fields had both a wider range and a higher median value of total MU when compared with the overall distribution of total MU for PBS fields. DCS, dynamic collimation system; MU, monitor units; PBS, pencil beam scanning.

however, both sets of measurements were similarly high with median gamma pass rates at 99.0% (PBS) and 98.3% (DCS), well above the 90% threshold acceptance criteria. Additionally, the number of unique trimmer positions did not appear to impact gamma pass rate among DCS deliveries (see Figure 7b), suggesting that the increase in plan complexity introduced with the trimmers does not have a strong effect on plan deliverability or TPS accuracy. Only a single measurement failed to meet the 90% passing threshold. This may be attributed to the high degree of modulation caused by using MFO techniques to generate the plans. Highly modular fields often had narrow regions of high dose and low dose gradient, limiting the depths that were suitable for measurement. Measurements obtained outside of this region were observed to have lower gamma pass rates (see Figure 10).

The increase in total MU observed in DCS deliveries was expected because the decrease in fluence for collimated spots necessitated higher beam-on times to deliver the same amount of dose. However, the increase in MU for a given patient was not uniform. When examined on a per-beam basis, the difference in MU between PBS and DCS beams varied. The variation in MU between beams may be partially attributed to the MFO optimization; using a single-field optimized (SFO) approach would likely result in more stability in MUs between beams. Although the median value of MU per field was higher for DCS deliveries, the difference was not statistically significant.

Although delivery times were higher for DCS plans compared to their PBS counterparts, the final time penalty observed during this study is not expected to be representative of a typical DCS delivery. HT does not currently include the spot position or trimmer position optimization that was present in the in-house TPS used in previous treatment planning studies with the DCS.[22] Instead, spot and trimmer positions are geometrically determined during initialization (see Section 2.2). During delivery optimization, wherein spots with similar trimmer positions are grouped together to improve delivery efficiency, it was observed that an aggressive optimization of delivery time returned smaller numbers of unique trimmers and resulted in plans of lower quality due to sub-optimal placement of spots/trimmers. To avoid this, the total number of unique trimmer positions was kept higher than would be used with fully optimized spot/trimmer positions to maintain a reasonable plan quality at the cost of higher plan delivery time (see Figure 7b). The addition of spot and trimmer position optimization algorithms in HT is expected to improve delivery time efficiency to the extent that the final number of unique trimmer positions (and therefore delivery time) may be reduced with minimal effects on plan quality. Furthermore, the proposed optimization of delivery efficiency does not create more complex fields, but rather changes the delivery order of the spots to reduce trimmer motion and treatment time. Therefore, the PSQA results presented here are not expected to change with time-optimized spot sequences.

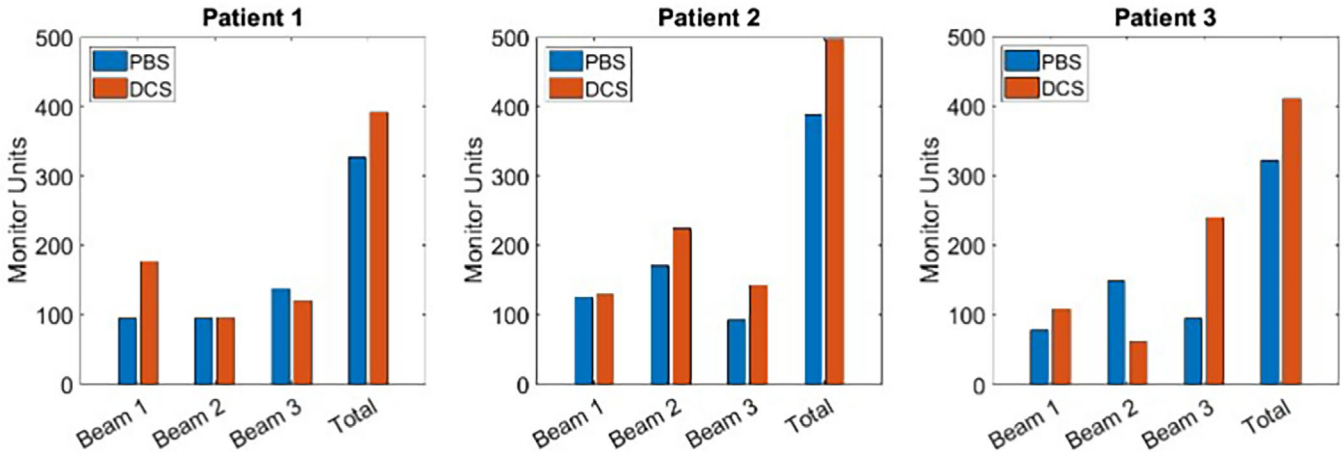

FIGURE 9 Per-beam and total MU for each patient. MU were generally higher for DCS beams compared to their PBS counterparts. Total MU, calculated as the sum of MU per beam across an entire plan, were always higher for DCS plans. DCS, dynamic collimation system; MU, monitor units; PBS, pencil beam scanning.

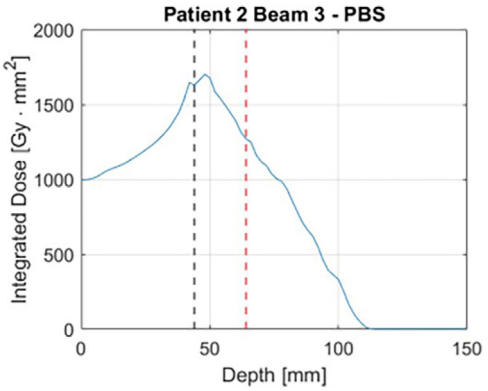

FIGURE 10 Lower gamma pass rates tended to occur for measurements obtained in high dose gradient regions. For Patient 2, the high degree of modulation of the field meant that the region of high dose and low dose gradient was narrow, limiting the depths for which measurement was suitable. The measurement obtained at 44 mm depth (black dashed line) passed with 94% of points exceeding the 3%/3 mm criteria; however, the measurement at 64 mm depth failed with only 88% of sampled points passing due to the high gradient observed at that depth (red dashed line).

5 | CONCLUSIONS

We have experimentally validated a PSQA process that is applicable to both standard PBS and dynamically collimated proton therapy. Additionally, we have shown that the DCS is capable of delivering plans of equal or higher conformity compared to PBS without sacrificing deliverability or accuracy.

ACKNOWLEDGMENTS

Research reported in this manuscript was supported by the National Cancer Institute of the National Institutes of Health under award number R37CA226518. Daniel E. Hyer, Ryan T. Flynn, and Patrick M. Hill are co-inventors on a patent that has been licensed to IBA.

CONFLICT OF INTEREST STATEMENT

The authors declare no conflicts of interest.

REFERENCES

1. Jones DTL, Schreuder AN. Magnetically scanned proton therapy beams: rationales and principles. *Radiat Phys Chem*. 2001;61:615-618.
2. Dinh J, Stoker J, Georges RH, et al. Comparison of proton therapy techniques for treatment of the whole brain as a component of craniospinal radiation. *Radiat Oncol*. 2013;8:289.
3. Zhang X, Li Y, Pan X, et al. Intensity-modulated proton therapy reduces the dose to normal tissue compared with intensity-modulated radiation therapy or passive scattering proton therapy and enables individualized radical radiotherapy for extensive stage IIIB non-small-cell lung cancer: a virtual clinical study. *Int J Radiat Oncol*. 2010;77:357-366.
4. Kase Y, Yamashita H, Fuji H, et al. A treatment planning comparison of passive-scattering and intensity-modulated proton therapy for typical tumor sites. *J Radiat Res*. 2012;53:272-280.
5. Moteabbed M, Yock TI, Depauw N, Madden TM, Kooy HM, Paganetti H. Impact of spot size and beam-shaping devices on the treatment plan quality for pencil beam scanning proton therapy. *Int J Radiat Oncol Biol Phys*. 2016;95:190-198.
6. Wang D, Dirksen B, Hyer DE, et al. Impact of spot size on plan quality of spot scanning proton radiosurgery for peripheral brain lesions. *Med Phys*. 2014;41(12):121705.
7. Hyer DE, Hill PM, Wang D, Smith BR, Flynn RT. Effects of spot size and spot spacing on lateral penumbra reduction when using a dynamic collimation system for spot scanning proton therapy. *Phys Med Biol*. 2014;59:N187-N196.
8. Hyer DE, Hill PM, Wang D, Smith BR, Flynn RT. A dynamic collimation system for penumbra reduction in spot-scanning proton therapy: proof of concept. *Med Phys*. 2014;41(9):091701.
9. Geoghegan TJ, Nelson NP, Flynn RT, Hill PM, Rana S, Hyer DE. Design of a focused collimator for proton therapy spot scanning using Monte Carlo methods. *Med Phys*. 2020;47(7):2725-2734. doi:10.1002/mp.14139
10. Smith BR, Hyer DE, Hill PM, Culberson WS. Secondary neutron dose from a dynamic collimation system during intracranial pencil beam scanning proton therapy: a monte carlo investigation. *Int J Radiat Oncol Biol Phys*. 2019;103:241-250.
11. Moignier A, Gelover E, Wang D, et al. Improving head and neck cancer treatments using dynamic collimation in spot scanning

proton therapy. *Int J Part Ther*. 2016;2(4):544-554. doi:10.14338/IJPT-15-00026.1
12. Moignier A, Gelover E, Wang D, et al. Theoretical benefits of dynamic collimation in pencil beam scanning proton therapy for brain tumors: dosimetric and radiobiological metrics. *Int J Radiat Oncol Biol Phys*. 2016;95:171-180.
13. Moignier A, Gelover E, Smith BR, et al. Toward improved target conformity for two spot scanning proton therapy delivery systems using dynamic collimation. *Med Phys*. 2016;43:1421-1427.
14. Smith B, Gelover E, Moignier A, et al. Technical note: a treatment plan comparison between dynamic collimation and a fixed aperture during spot scanning proton therapy for brain treatment. *Med Phys*. 2016;43:4693-4699.
15. Nelson NP, Culberson WS, Hyer DE, et al. Dosimetric delivery validation of dynamically collimated pencil beam scanning proton therapy. *Phys Med Biol*. 2023;68:055003.
16. Nelson NP, Culberson WS, Hyer DE, et al. Integration and dosimetric validation of a dynamic collimation system for pencil beam scanning proton therapy. *Biomed Phys Eng Express*. 2023;9:065024.
17. Bennett LC, Hyer DE, Erhart K, et al. PETRA: a pencil beam trimming algorithm for analytical proton therapy dose calculations with the dynamic collimation system. *Med Phys*. 2023;50:7263-7280.
18. Mayo C, Martel MK, Marks LB, Flickinger J, Nam J, Kirkpatrick J. Radiation dose-volume effects of optic nerves and chiasm. *Int J Radiat Oncol Biol Phys*. 2010;76:S28-S35.
19. Lawrence YR, Li XA, El Naqa I, et al. Radiation dose-volume effects in the brain. *Int J Radiat Oncol Biol Phys*. 2010;76:S20-S27.
20. Paddick I, Lippitz B. A simple dose gradient measurement tool to complement the conformity index. *J Neurosurg*. 2006;105:194-201.
21. Gorissen BL. Guaranteed ε-optimal solutions with the linear optimizer ART3+O. *Phys Med Biol*. 2019;64:075017.
22. Smith BR, Hyer DE, Flynn RT, Culberson WS. Technical note: optimization of spot and trimmer position during dynamically collimated proton therapy. *Med Phys*. 2019;46:1922-1930.
23. Smith BR, Hyer DE, Flynn RT, Hill PM, Culberson WS. Trimmer sequencing time minimization during dynamically collimated proton therapy using a colony of cooperating agents. *Phys Med Biol*. 2019;64(20):205025. doi:10.1088/1361-6560/ab416d
24. Arjomandy B, Sahoo N, Ciangaru G, Zhu R, Song X, Gillin M. Verification of patient-specific dose distributions in proton therapy using a commercial two-dimensional ion chamber array. *Med Phys*. 2010;37:5831-5837.
25. Chang C, Poole KL, Teran AV, Luckman S, Mah D. Three-dimensional gamma criterion for patient-specific quality assurance of spot scanning proton beams. *J Appl Clin Med Phys*. 2015;16:381-388.
26. Magro G, Fassi M, Mirandola A, et al. Dosimetric validation of a GPU-based dose engine for a fast in silico patient-specific quality assurance program in light ion beam therapy. *Med Phys*. 2022;49:7802-7814.
27. Zhu X, Li Y, Mackin D, et al. Towards effective and efficient patient-specific quality assurance for spot scanning proton therapy. *Cancers*. 2015;7:631-647.
28. Miften M, Olch A, Mihailidis D, et al. Tolerance limits and methodologies for IMRT measurement-based verification QA: recommendations of AAPM task group no. 218. *Med Phys*. 2018;45:e53-e83.
29. Ates O, Pirlepesov F, Zhao Li, Hua C-H, Merchant TE. Development of a log file analysis tool for proton patient QA, system performance tracking, and delivered dose reconstruction. *J Appl Clin Med Phys*. 2023;24:e13972.
30. Chen M, Yepes P, Hojo Y, et al. Transitioning from measurement-based to combined patient-specific quality assurance for intensity-modulated proton therapy. *Br J Radiol*. 2020;93:20190669.
31. Hernandez Morales D, Shan J, Liu W, et al. Automation of routine elements for spot-scanning proton patient-specific quality assurance. *Med Phys*. 2019;46:5-14.
32. Mackin D, Zhu XR, Poenisch F, et al. Spot-scanning proton therapy patient-specific quality assurance: results from 309 treatment plans. *Int J Part Ther*. 2014;1(3):711-720. doi:10.14338/IJPT-14-00017.1
33. Shalabh. Nonparametric statistical inference. *J R Stat Soc Ser A Stat Soc*. 2011;174:508-509.
34. Lin L, Kang M, Solberg TD, et al. Use of a novel two-dimensional ionization chamber array for pencil beam scanning proton therapy beam quality assurance. *J Appl Clin Med Phys*. 2015;16:270-276.
35. Rawiwan N, Chatchumnan N, Vimolnoch M, Kingkaew S, Oonsiri S. Patient-specific quality assurance in pencil beam scanning by 2-dimensional array. *Int J Part Ther*. 2023;10:105-110.

How to cite this article: Bennett LC, Hyer DE, Vu J, et al. Patient-specific quality assurance of dynamically-collimated proton therapy treatment plans. *Med Phys*. 2024;1-10. https://doi.org/10.1002/mp.17295